

# Robust Detection and Visualization of Jet-stream Core Lines in Atmospheric Flow

Michael Kern, Tim Hewson, Filip Sadlo, Rüdiger Westermann, and Marc Rautenhaus

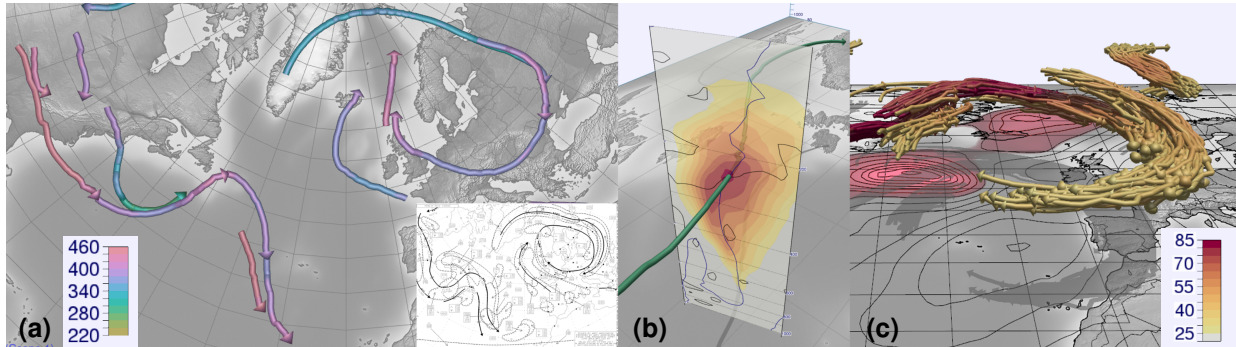


Fig. 1. (a) Jet-stream core lines extracted from a 3D wind field with our method, colored by flight level (hft). To the best of our knowledge, these features are still created manually by domain experts in operational weather forecasting and provided via 2D maps, as shown in the inset. (b) Normal plane perpendicular to the wind vector, used by our method as a local coordinate frame to extract jet cores. Color shows wind speed ( $\text{ms}^{-1}$ ). (c) 3D “spaghetti plot” visualization of an ensemble of jet-stream cores (color shows wind speed as in (b)) enables an improved analysis of their spatial structure, forecast uncertainty, and relation to further atmospheric features including, e.g., mean-sea level pressure (MSLP; black contour lines, red regions indicate where pressure is below 1000 hPa).

**Abstract**— Jet-streams, their core lines and their role in atmospheric dynamics have been subject to considerable meteorological research since the first half of the twentieth century. Yet, until today no consistent automated feature detection approach has been proposed to identify jet-stream core lines from 3D wind fields. Such 3D core lines can facilitate meteorological analyses previously not possible. Although jet-stream cores can be manually analyzed by meteorologists in 2D as height ridges in the wind speed field, to the best of our knowledge no automated ridge detection approach has been applied to jet-stream core detection. In this work, we—a team of visualization scientists and meteorologists—propose a method that exploits directional information in the wind field to extract core lines in a robust and numerically less involved manner than traditional 3D ridge detection. For the first time, we apply the extracted 3D core lines to meteorological analysis, considering real-world case studies and demonstrating our method’s benefits for weather forecasting and meteorological research.

**Index Terms**—Meteorology, weather forecast, jet-stream, feature detection

## 1 INTRODUCTION

The improvement of weather forecasts and climate change projections depends heavily on documenting and understanding complex three-dimensional structures in the atmosphere. A key component of those structures is the jet-stream. Jet-streams are regions of high wind speed, typically encountered near to the top of our principal weather systems, at altitudes of about 8-16km. As well as determining the general weather type—such as blocking and storm tracks—they also exert a strong dynamical influence on severe weather events, such as extreme windstorms [2]. Jet-streams are also related to clear-air turbulence (CAT), important for daily aviation operations. In this respect, jet-stream core lines—lines of maximum wind speed—are operationally depicted as fundamental atmospheric structures on significant weather (SIGWX) charts used by pilots [53]. Even though a concise definition of jet-streams has long been provided by the World Meteorological Organization (WMO) [54], jet-stream core lines in operational weather

forecast settings are, similar to other atmospheric features including fronts, still identified manually. This process is time-consuming, requires expertise, and does not allow for a full analysis of the 3D geometry of the jet-stream core lines and how this relates to features of the surrounding atmosphere.

In this article, we approach the still unsolved question of how jet-stream core lines can be objectively identified from three-dimensional numerical weather prediction (NWP) data in an automated, robust manner, and visualized in a way that can benefit a subsequent in-depth meteorological analysis of the model atmosphere.

### 1.1 Problem Description

A jet-stream is officially defined by the WMO as a “flat tubular, quasi-horizontal, current of air generally near the tropopause, whose axis is along a line of maximum speed and which is characterized by great speeds and strong vertical and horizontal wind shears” [54]. Its core line is defined as the “line along which the wind speeds are maximum both in the vertical and in the horizontal” [54]. Yet in spite of the pivotal role that jet-streams and their core lines play, as a driving force in atmospheric dynamics, we are unaware of any objective three-dimensional identification methodology built on this definition that can be applied in a practical way to meteorological analysis.

Such automated detection and visualization of jet-stream core lines is much needed because of the following:

- Using a single 3D visualization, with a fly-through capability, it

- Michael Kern, Rüdiger Westermann and Marc Rautenhaus are with the Computer Graphics & Visualization Group, Technische Universität München, Garching, Germany. E-mail: {michi.kern, westermann, marc.rautenhaus}@tum.de
- Tim Hewson is with the European Centre for Medium-Range Weather Forecasts, Reading, UK. E-mail: tim.hewson@ecmwf.int
- Filip Sadlo is with the Visual Computing Group, Heidelberg University, Heidelberg, Germany. E-mail: sadlo@uni-heidelberg.de

would provide a greatly increased capacity to understand the key relationships and dependencies between multiple atmospheric processes and the jet.

- It would provide a new way of understanding and critically assessing the uncertainty inherent in ensemble forecasts, and notably occasions when there is insufficient spread, that results in ‘forecast busts’ around the world. Jet-stream behavior is implicated in studies of these forecast failures.
- Automated core-line extraction is much needed to assist with the generation of SIGWX charts for aviation; currently the manual procedure relies heavily on representation of a single jet level.

A specific unsolved issue in meteorology that can benefit from automated jet-stream core detection and for which we discuss the application of our method is the modulation of the jet-stream by other atmospheric processes and the influence of such modulation on the predictability of downstream weather. Specific examples for such processes include extreme convection over the United States [41], and Warm Conveyor Belts (WCBs, airstreams in extratropical cyclones that lift warm and moist air from near the surface to the upper troposphere; e.g., [7]) over the north Atlantic, which can both modulate the jet-stream and cause large uncertainties in predictions for European weather.

## 1.2 Contribution

The jet-stream core line definition provided by the WMO relates to the definition of three-dimensional height ridges encountered in different contexts in flow visualization [48], [46], [43]. Yet, while a number of studies in meteorology have proposed methods to detect –mainly two-dimensional– jet-stream features (cf. Sect. 2), to the best of our knowledge no ridge detection method has been applied to the automated extraction of 3D jet-stream core lines.

In this work, we propose a robust 3D detection method for jet-stream core lines in NWP data that directly reflects the official WMO definition and that relates to height ridge computation. By exploiting the fact that jet-stream core lines are at very narrow angles to the wind direction and the fact that the vertical wind component is negligible compared to the horizontal in large-scale atmospheric flow, we can determine the core lines as wind speed maxima in vertical planes perpendicular to the horizontal wind direction. Thus, in contrast to “classical” ridge detection algorithms, which determine maxima in vertical planes spanned by the eigenvectors of the 3D Hessian matrix, our approach does not suffer from spurious variations due to noise, and it can be enforced explicitly that the planes are consistently oriented. As a consequence, the jet cores extracted by our method are more robust, i.e., less disjointed and cluttered. Furthermore, our method does not require excessive blurring of the underlying field and can work on the original data. Fig. 2 demonstrates the differences in the extracted jet cores using both methods.

We integrate our new detection method into the interactive 3D meteorological ensemble visualization tool “Met.3D” [38], facilitating combination of the detected features with further atmospheric visualizations, and propose a number of visualizations of the core lines that help with the analysis of NWP data to investigate the motivating meteorological research questions. In particular, we visualize

- 3D jet-stream core lines in combination with 3D depictions of atmospheric processes including clouds,
- 3D spaghetti plots of jet-stream core lines extracted from ensemble weather forecasts to depict forecast uncertainty with respect to the jets,
- the relation of the core lines to local streamlines and surrounding atmospheric conditions (such as cloud water content or surface pressure),
- an automated SIGWX jet-stream product.

We apply the proposed techniques to analysis of NWP data from the European Centre for Medium-Range Weather Forecasts (ECMWF), demonstrating insight that can be gained regarding the posed meteorological research questions.

## 2 RELATED WORK

Our work relates to research connected to jet-streams and their detection in the atmospheric sciences, and to the extraction of line features in flow visualization. Concerning the latter, ridge detection is of particular importance.

### 2.1 Jet-stream Detection

Major references for jet-streams and their characteristics, including previous research and a description of manual analysis methods, date back to the books by Reiter [39] and Palmen and Newton [34]. Here, the jet-stream axis on a 2D chart was introduced as the “line of maximum wind speed”. The “layer of maximum wind” (LMW) was introduced as a method to analyze the 3D jet-stream axis (=core). The LMW was operationally used for weather forecasting in the U.S. (cf. [49]) and is also utilized today in operational production of SIGWX charts (Sect. 5.1).

Automatic extraction of jet-streams has been mainly investigated in the past 15 years, primarily to compile climatologies. Some authors try to identify core lines, others simply use speed thresholds. Often the classification of a model grid point as belonging to a jet-stream has been considered sufficient. Also, studies commonly look first for the maximum wind in the vertical, as in the LMW concept.

Koch et al. [20] counted events for each horizontal grid point where the average wind speed between 100 and 400 hPa exceeds a threshold, whilst Archer and Caldeira [1] used mass-flux weighted averages to determine jet-stream events per horizontal grid point. Similar height-dependent thresholding on wind speed was used by Limbach et al. [23] and Martius [31]. Meanwhile Schiemann et al. [45], Pena-Ortiz et al. [36] and Barton and Ellis [3] compute jet-stream core events in various ways, but with the common assumption that jets must propagate west to east. Also for the purpose of a climatology, Gallego et al. [12] defined a criterion based on a geostrophic streamline of maximum average velocity to get jet-like streamlines circumventing the southern hemisphere.

Strong and Davis [49–51] used a notion similar to the LMW. The core is detected on their LMW equivalent by computing wind speed maxima via finite differencing in the y-direction only. However line geometry was not used. Manney et al. [29,30] constructed a climatology of jet-stream cores by cataloging wind speed maxima on longitudinal cross-sections (no detected line geometry). More recently, Molnos et al. [32] introduced a network-based scheme using shortest paths to detect jet-stream core as a continuous, globe-circumventing line. The method is calibrated using an image-based jet analysis technique by Rikus [40], and used to compute frequencies of jet-core occurrence. Recently, Spensberger et al [47] adapted a 2D criterion by Berry et al. [4] to 2D wind fields on a “dynamical tropopause”, an isosurface of 2 PV (potential vorticity) units.

Most of the above methods are not Galilean invariant. They mostly depend on assuming a priori that the jet-stream exhibits certain characteristics; for example that it is westerly. In contrast, the methodology in this paper, which follows on principally from techniques described in Berry et al (2007), is Galilean invariant, and will identify jet-streams equally in all directions and at all atmospheric levels.

### 2.2 Line Features in Fluid Dynamics / Flow Visualization

Feature extraction is an important tool and an active branch of research in flow visualization. A particular reason for its importance is the comparably high dimensionality of vector fields—they add the difficulty of three-dimensional range visualization to the already difficult representation of three spatial and one temporal dimensions of their domain. The fact that flow fields, which are a primary source for vector fields, tend to exhibit turbulence and chaotic advection further complicates their analysis, necessitating effective visualization approaches with as few parameters as possible.

Line-type features are particularly useful for this purpose due to several reasons: they are able to give a concise picture of flow fields, do not suffer from occlusion, and there are many variants that are conceptually free of parameters. A widely used and very successful line feature in flows is the vortex core lines. As no general definition of a vortex has been found so far, there exist also several competing definitions for vortex core lines. A vortex core line can be seen as the (possibly bent) axis of vortical fluid motion, representing the set of points around which massless particles in the flow swirl. A widely used definition for vortex core lines is that by Sujudi and Haimes [52]. Peikert and Roth [35] presented a mathematical framework, the parallel vectors operator, in which Sujudi and Haimes' definition can be formulated as the loci where the real eigenvector of the Jacobian of the vector field is parallel to the flow vector, with the additional requirement of the other two eigenvalues being complex. An other prominent vortex core line definition is that by Levy et al. [22], which, in this framework, requires the vorticity vector to be parallel to velocity. The parallel vectors operator, representing line-type features in general as the locations where two (derived) vector fields are parallel or anti-parallel, can also be used for defining separation lines and attachment lines [18], and the related bifurcation lines [27, 42].

In scalar fields, a prominent line-type feature is that of ridges and valleys. Ridges and valleys can be interpreted as generalized local extrema. Local extrema in  $n$ -dimensional scalar fields can be defined as points which exhibit a respective extremum in  $n$  orthogonal profile sections cutting through that point. If we relax this condition by one dimension, i.e., taking the set of points at which only  $n - 1$  orthogonal profile sections exhibit a local maximum (minimum), we obtain ridge (valley) lines. In early work in the context of surface topography, ridges and valleys were first mathematically described and idealized [5, 8]. Ridge extraction (we imply here also valleys, since valleys can be obtained by extracting ridges from the negated field) is widely applied in image analysis and computer vision, with a digital image treated as a scalar field. Ridges serve as characteristic structures in these domains, complementary to edges, within the boundaries of objects [14, 24, 28]. For ridge surfaces, i.e., where only one profile section has to exhibit a local maximum, Furst and Pizer [11] presented an approach for their extraction from 3D scalar fields, by tracing them through the volume. Ridge surfaces were applied to volumetric data by Kindlmann et al. [19] to visualize diffusion tensor MRI data. In the context of flow visualization, ridges have become a common tool to indicate and extract, e.g., vortex core lines [48], flow separation [46], by Sahner et al. [44] to visualize vorticity and strain, and by Sadlo et al. [43] to display separating regions of different flow behavior in unsteady vector fields. Peikert et al. [35] described an efficient and alternative way to compute and filter height ridges with an implicit formulation with respect to the eigenvectors of the Hessian.

### 2.3 Ridge Detection

A widely used formulation for ridges is that of height ridges by means of the gradient and the Hessian of a scalar field. Let  $s(\vec{x})$  be the 3D scalar field where we want to extract ridge lines from. Height ridge lines according to Eberly [10] are defined by the parallel vectors operator as the loci where

$$\nabla s(\vec{x}) \parallel \vec{e}_3, \quad (1)$$

i.e., where the major eigenvector  $\vec{e}_3$  of the Hessian  $\nabla \nabla s(\vec{x})$  and the gradient of the scalar field are (anti-)parallel, with the additional condition that the two other eigenvalues need to be negative:

$$\lambda_1 < 0, \quad \text{and} \quad \lambda_2 < 0, \quad (2)$$

with  $\lambda_1 \leq \lambda_2 \leq \lambda_3$ , and  $\vec{e}_i$  being the eigenvector for eigenvalue  $\lambda_i$ .

In this formulation,  $\vec{e}_3$  is considered parallel to the ridge line tangent, and  $\vec{e}_1$  and  $\vec{e}_2$  perpendicular to it (note that the eigenvectors form an orthonormal system because the Hessian is symmetric). That is, we can consider  $\vec{e}_1$  and  $\vec{e}_2$  being normal vectors to the ridge line. One difficulty with this assumption is that it is typically never exactly met in practice. The angle  $\alpha$  between the (anti-)parallel vectors  $\nabla s(\vec{x})$  and  $\vec{e}_3$ , and the feature tangent is, for well-defined ridges, commonly larger

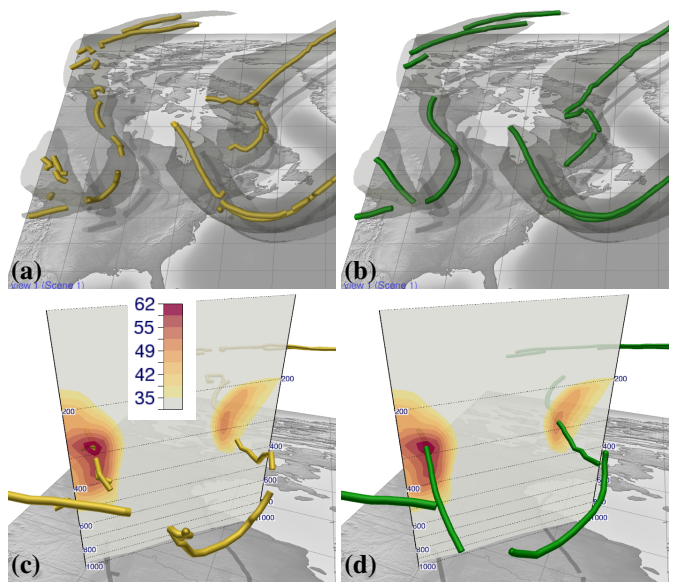


Fig. 2. 3D visualizations of maxima lines extracted from a 3D wind field. Shown are extracted lines via (a) the “classical” 3D ridge detection algorithm (yellow polylines) and (b) via our proposed method (green), restricted to regions with a wind speed of at least  $40 \text{ ms}^{-1}$  (enclosed by the dark-greyish isosurface). (c) Two maxima depicted by the contour lines of windspeed (color shows windspeed in  $\text{ms}^{-1}$ ) in a vertical section are not properly detected by ridge detection. (d) Our method robustly extracts jet cores even where ridge detection fails.

than 25 degrees. Peikert and Roth [35] use  $\alpha$  as a quality criterion for extracted ridge lines, and filter their regions by imposing an upper threshold on this value, i.e., rejecting ridge line parts where this angle exceeds the threshold. It is not uncommon that the threshold needs to be set above 45 degrees to obtain useful results in practical data, which means that the eigenvectors may switch role regarding their “orthogonality” to the line feature tangent. An involved difficulty is that the gradient and the Hessian need to be estimated from the data, suffer from amplification of noise, and that obtaining smooth and at the same time interpolation-consistent derivatives is a difficult and often, as in the case of trilinear interpolation, impossible undertaking. All in all, although useful and widely employed, height ridges by means of eigenvectors of the Hessian tend to suffer with respect to robustness, false positives, and false negatives (disruptions)—often impeding effective visualization (compare Fig. 2). A main reason for these issues is the instability of the eigenvectors of the Hessian with respect to the aimed ridge line feature.

In this work, we present, for the special case of scalar fields derived from vector fields, as is the case for jet-stream cores, an approach that avoids the computation of the Hessian except for masking purposes. Instead, we derive the required two normal directions across the ridge line from the vector field itself—and although these are, in general, also not strictly perpendicular to the resulting feature line, they are as continuous as the vector field—leading to superior results.

## 3 DETECTION METHOD

### 3.1 Definition and Assumptions

Based on the WMO definition, we define and interpret jet cores as follows: A jet core is a core of fluid having higher momentum than its surroundings. By examining the plane perpendicular to the momentum vector at every point in space, one can ascertain whether each point belongs to a jet core. In large-scale meteorology, momentum in the vertical plane is negligible. Therefore, jet cores lie in an approximately horizontal plane, and, thus, the normal planes are always vertical. If within its normal plane a point is a local maximum in resolved mo-

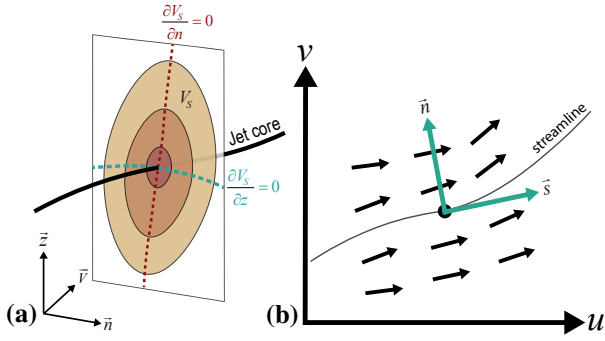


Fig. 3. (a) Sketch of the normal plane at a jet core intersection point. On the normal plane, colored contours of wind speed  $V_s$  (low speeds are yellow, high speeds red) are shown. The cyan (red) dotted line shows where the vertical (horizontal) derivative along the plane is zero. The jet core crosses the plane at the intersection of these zero lines. (b) Illustration of the local coordinate system in the 2D wind vector field used to construct the normal plane.  $\vec{s}$  is the unit vector tangential to the current streamline,  $\vec{n}$  is normal to it.

mentum then it belongs to a jet core. The connection of all maxima points form the jet core lines. In an NWP model, the momentum  $p$  per grid point is defined as  $p = \rho \vec{v}$ , where  $\rho$  denotes the density and  $\vec{v}$  the velocity (or wind vector), both changing over time. Since we assume that the density  $\rho$  of the air is locally constant the resolved momentum at each grid point is maximal if the wind speed  $|\vec{v}|$  is maximal within its normal plane. Fig. 3 illustrates the definition.

In our mathematical definition of jet cores we are employing the notion of following lines along which there is both zero horizontal and vertical shear. On a jet axis there is zero shear vorticity (as in [4]). And similarly in the vertical there is zero (speed) shear in parallel components. Additional masking is applied to further eliminate all wind speed minima and light wind conditions in general (also following [4]).

### 3.2 Data

We use NWP data from the ensemble prediction component (ENS) of the ECMWF Integrated Forecast System (IFS) (e.g., [21]), which comprises 50 perturbed members and an unperturbed control forecast. Data are available on a regular longitude–latitude grid in the horizontal, whilst in the vertical terrain-following hybrid sigma–pressure coordinates are used [37]. In this work, we use ECMWF ENS forecasts initialized at 00:00 UTC, 22 and 25 September 2016.

The output 3D wind vector  $\vec{v} = (u, v, \omega)$ , defined at grid points in longitude–latitude–pressure space, is composed of the horizontal wind-components  $u$  (eastward wind) and  $v$  (northward wind) defined in meters per second ( $\text{ms}^{-1}$ ), and  $\omega$  (vertical wind) defined in Pascals per second ( $\text{Pa s}^{-1}$ ).  $\omega$  can be approximately converted to  $\text{ms}^{-1}$ , however, its order of magnitude is significantly smaller than that of the horizontal wind:  $\mathcal{O}(0.05 \text{ ms}^{-1})$  compared to  $\mathcal{O}(50 \text{ ms}^{-1})$ . The vertical wind component thus has a negligible impact on both direction and magnitude of the 3D wind vector, we can hence ignore  $\omega$  for jet core detection.

### 3.3 Mathematical Framework

Based on the official WMO definition and our understanding of jet cores in atmospheric flow, we elaborated a framework to mathematically define jet core lines in NWP model data. With these equations, we are able to robustly compute candidate points for jet cores and extract three-dimensional curve lines representing the jet-stream cores from a volumetric, gridded wind vector field.

Our method is built upon the notion of maxima ridges in 3D wind fields, i.e., we are aiming for the detection of local maxima points along a local coordinate frame (the normal plane) perpendicular to the current velocity vector. In principal, we have done so by following “classical” ridge extraction techniques. However, we found that computing eigenvectors in real-world 3D data sets tends to be unstable, resulting

in jet cores that are commonly disjointed and cluttered (see Fig. 2 for a comparison). To avoid this, we introduce an alternative approach that, under the assumptions we make, can extract jet cores well aligned with those analyzed in operational weather forecasting, yet in a far more stable way.

Our method employs a fixed local frame-of-reference (Fig. 3) to locate our candidate points for the final jet core lines. As such it builds on the approach adopted by [15] to identify atmospheric front lines objectively, and [4] who identify 2D trough axes and 2D jet cores. Consider a local coordinate system  $(\vec{s}, \vec{n})$  at a grid point  $X$ , where  $\vec{s}$  is parallel to the local 2D (horizontal) wind vector  $\vec{V} = (u, v)$ , and  $\vec{n}$  is normal to it. Then, the horizontal wind vector at each grid point can be split into two constituent components:  $\vec{V} = (u, v) \equiv (V_s, V_n)$  where  $V_s$  is the wind speed along the vector  $\vec{s}$  and  $V_n$  is the wind speed along  $\vec{n}$ . The magnitude  $V$  of the wind vector at  $X$  is  $V = |\vec{V}| = V_s$ , since  $\vec{V}$  is parallel to  $\vec{s}$  and  $V_n$  is locally zero.

For each grid point surrounding  $X$ , let  $V_s$  be the magnitude of the local wind vector resolved into direction  $\vec{s}$ . The jet-stream core colocalizes with lines along which  $V_s$  is maximal within the local two-dimensional normal planes spanned by  $\vec{n}$  and  $\vec{z}$ . This is given if the derivatives in the horizontal and vertical direction are both locally zero:

$$\frac{\partial V_s}{\partial n} = 0 \quad (3) \quad \frac{\partial V_s}{\partial z} = 0 \quad (4)$$

These equations denote three-dimensional contorted isosurfaces (of zero shear vorticity), where the quasi-vertical isosurface is described by Eq. 3 and the quasi-horizontal sheet is described by Eq. 4. The set of all extremum points in 3D-space, which are considered the potential candidate points for the jet cores, is defined by the intersection of these two isosurfaces. Connections of these candidate points resemble polylines in 3D-space. We are interested in regions of high wind speeds, usually above about  $40 \text{ ms}^{-1}$ ; therefore, core lines detected in light wind conditions need to be removed. We hence add an inequality mask (Eq. 5) to Eqs. 3 and 4 to focus on high wind speeds (this also helps to circumvent noise). For a given threshold  $\alpha$  (in  $\text{ms}^{-1}$ ) each candidate point has to satisfy:

$$V_s > \alpha \quad (5)$$

From all extremum points that are candidates for the jet cores we need to filter out all those that are a local minimum or a saddle point. The type of the extremum point within the  $\vec{n}$ – $\vec{z}$ -plane (local “normal plane”) can be determined by the local Hessian matrix and the sign of its corresponding eigenvalues. The Hessian matrix  $H_N$  within the local normal plane coordinate frame is defined as follows:

$$H_N = \begin{bmatrix} \frac{\partial^2 V_s}{\partial n^2} & \frac{\partial^2 V_s}{\partial n \partial z} \\ \frac{\partial^2 V_s}{\partial z \partial n} & \frac{\partial^2 V_s}{\partial z^2} \end{bmatrix} \quad (6)$$

Given the Hessian matrix  $H_N$ , a line point is said to be a local (convex/elliptic) maximum if the sign of both eigenvalues is negative. Hence, an additional mask is applied to all line points to extract only those where the following inequalities hold:

$$\lambda_0 < 0, \lambda_1 < 0 \quad (7)$$

The computed eigenvalues  $\lambda_i$  are real since the Hessian matrix  $H_N$  is symmetric.

The major difference to ridge extraction techniques working directly on the 3D wind field is that our technique works in a fixed reference frame. Thus, we avoid working in the eigenvector-frame for both the computation of first and second order derivatives, and we can thereby avoid oscillations –due to oscillating eigenvectors– in the frame of reference for the first derivatives. This makes the technique significantly more robust for jet core extraction. Indeed this local coordinate-based mechanism for noise removal aligns closely with the mechanism used in [15] to eliminate third-derivative noise during front detection (see his Figure 6).

### 3.4 Feature Extraction

We now describe the numerical computations involved to extract jet cores from 3D gridded wind fields.

#### 3.4.1 Raw Features

We call the set of candidate points that satisfy Eqs. 3 and 4 “raw features” that potentially belong to a jet core. To extract raw features, we first compute the directional (horizontal) and vertical derivatives in 3D-space at every grid point  $X$ : First, the local coordinate frame  $(\vec{s}, \vec{n})$  is derived at  $X$  by using the unit vector parallel to the local horizontal wind vector and computing the orthogonal normal vector. Second, the local wind vectors at surrounding grid points are projected onto  $\vec{s}$ .

To solve Eq. 3, the directional derivative into direction  $\vec{n}$ , we apply the chain rule to obtain

$$\frac{\partial V_s}{\partial n} = (\vec{n} \cdot \vec{\nabla}) V_s = n_x \frac{\partial V_s}{\partial x} + n_y \frac{\partial V_s}{\partial y}. \quad (8)$$

The partial derivatives are computed using finite differences, taking care of the geometric distance between two grid points in  $x$  and  $y$ -direction. As  $V_s$  is defined in  $\text{ms}^{-1}$  and the horizontal grid is defined in longitude–latitude space, we need to ensure consistency in the used distance metric. While the distance between two latitudinal points is constant over the globe at approximately 111 km per  $^\circ$ , the longitudinal distance decreases towards the poles. Assuming a spherical globe, it can be computed by scaling the equatorial distance (111 km per  $^\circ$ ) by the cosine of the latitude.

The vertical derivative (Eq. 4) is computed via finite differences at each grid point  $X$  at level  $k$  into the direction of  $\vec{z}$ , by using the resolved wind vectors of the surrounding levels. Here, the vertical position of each grid point defined in pressure space needs to be converted to geometric height (in m) first.

#### 3.4.2 Zero-Isosurface Crossing Extraction

A naive approach to compute the intersection of two isosurfaces implicitly defined in a 3D scalar field on a discrete voxel grid uses the Marching Cubes algorithm [26]. The triangle geometry of both isosurfaces is extracted, and per-voxel triangle intersection tests compute the intersection lines. Such an approach, however, would be very inefficient since we do not require the entire isosurface geometries but only the geometry of the raw line features.

We hence use the Marching Faces algorithm proposed by Ljung and Ynnerman [25] to implicitly extract intersection lines between two isosurfaces from two co-located scalar fields. Marching Faces traverses each voxel of a 3D grid and computes the intersection points of isosurface crossings at each voxel face, by computing crossings of the isolines of each isosurface at a face. Isolines are approximated by linear interpolation along the face edges (similar to Marching Squares), the crossing of two isolines is computed analytically.

Ljung and Ynnerman’s approach first identifies all intersection points per voxel face in parallel, then joins points sharing a common voxel face to create a polyline. We have modified this approach and in our method directly trace the polylines through the grid. We traverse the grid along subsequent voxels and combine points that share a common face; tracing is stopped if a voxel does not contain a suitable intersection point or a looped curve is detected.

### 3.5 Filtering

After raw features have been extracted, the resulting lines are filtered to obtain features that represent local maxima in wind speed. First, all candidate points of too low wind speed are removed by applying Eq. 5 to each raw feature vertex. Results from two different windspeed thresholds are shown in Fig. 4a ( $40 \text{ ms}^{-1}$ ) and b ( $10 \text{ ms}^{-1}$ ). A smaller threshold increases the number of jet core lines as well as their length. For the application cases in this work, the domain experts were interested in jet cores with a velocity of at least  $40 \text{ ms}^{-1}$ ; we use this threshold throughout this paper.

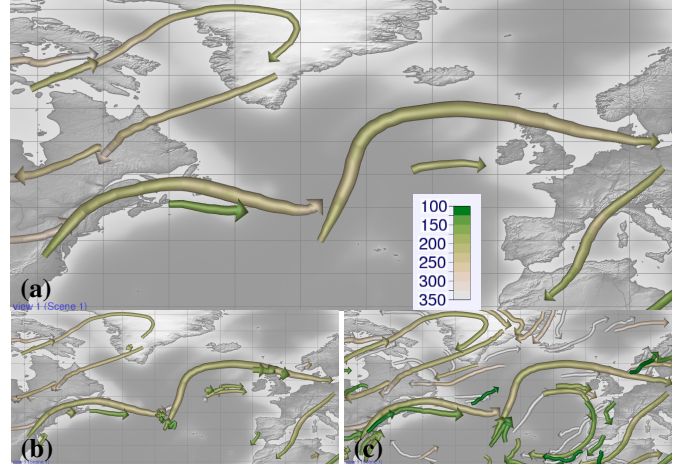


Fig. 4. 2D visualization of jet-stream core lines. (a) Core lines exceeding  $40 \text{ ms}^{-1}$ , filtered according to a minimum length of 500 km and a maximum angle of  $55^\circ$ . Tube thickness maps to the magnitude of the wind (thick lines indicate high wind speed), color maps to pressure elevation (colorbar in hPa, lower pressure corresponds to higher height). (b) Same as (a) but with length and angle filters disabled. (c) Same as (a) but with the wind speed threshold reduced to  $10 \text{ ms}^{-1}$  (length and angle filters enabled).

#### 3.5.1 Hessian Computation

To determine which raw feature points belong to a local maximum, i.e., where  $V_s$  is locally maximal in the  $\vec{n}$ - $\vec{z}$ -plane, we compute the Hessian matrix and its eigenvalues (Eq. 6) at each line vertex. Since the raw feature points are points in 3D-space and not located on the grid points, we compute the entries of  $H_N$  as follows: Second partial derivatives with respect to  $V_s$  are computed per grid point and are each stored in a separate grid. The second derivatives at a given line vertex are then obtained by tri-linear interpolation using the 8 grid points surrounding the vertex. As the Hessian matrix is approximated on a finite grid and its eigenvalues tend to oscillate, points can be falsely rejected (or accepted). Thus, we introduce a threshold  $\beta$  to soften the criterion in Eq. 7:  $\lambda_i < \beta$ , where  $\beta$  is a small positive value. Short line disconnections due to false rejections are in our method counteracted by a curve-following algorithm which keeps track of the eigenvalues along a core line. Falsely rejected points that are enclosed by two accepted points are subsequently corrected.

#### 3.5.2 Geometric Length

Aviation centers are generally interested in jet-stream cores that at least extend over a certain distance; these cores are expected to have more influence on surrounding atmospheric conditions than short jet cores. We compute the geometric length of each core line in kilometers and remove lines whose length is below a user-specified threshold. Fig. 4a and b shows the effect of this filter; as expected, more short jet cores are detected when the length filter is omitted. For the remaining figures in this paper, we set this threshold to 500 km; shorter jet cores often resulted from small maxima regions and did not contribute to the analysis.

#### 3.5.3 Angle Criterion

Numerical inaccuracies, in particular in regions in which the wind speed differences are small or the local maximum is ill-defined, can lead to misclassification of raw feature points, i.e., saddle or minima points are falsely detected as local maxima. These misclassified points can lie between two close jet cores and can be relocated to the same voxel. In such a case, our line tracing algorithm from Sec. 3.4.2 may combine the ends of two distinct lines so that the resulting jet cores can exhibit unphysical “bending”. To filter such cases, we determine a horizontal angle between each two core line segments and vertical pressure differences at the core line end segments, and apply filters to

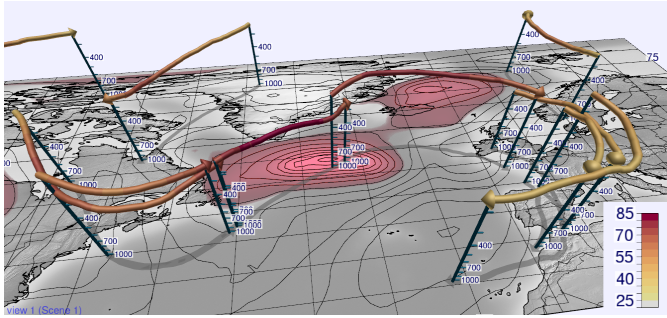


Fig. 5. Core lines rendered in 3D (colored by wind speed in  $\text{ms}^{-1}$ ). Shadows cast to the ground and vertical drop-lines (labeled by pressure in hPa) significantly improve spatial perception of the view. Black surface contour lines and red highlighted regions show MSLP as in Fig. 1, aiding the analysis of the relation of the jet cores to surface weather systems.

remove lines that exceed a user-defined angle or pressure difference threshold. Choosing high angle thresholds can result in more sharply bent core lines (especially in saddle point regions), as illustrated in Fig. 4c. For this work, we found thresholds of  $55^\circ$  and 10 hPa for angle and pressure, respectively, to yield good results in our examples.

### 3.6 Performance

Ljung and Ynnerman [25] showed the complexity of computing the intersection between two isosurfaces to be  $\mathcal{O}(\sqrt{N})$ , where  $N$  is the number of triangles in the isosurfaces (which in turn depends on grid dimensions and the characteristic of the considered scalar fields). Our subsequent filtering of the core line candidates is of order  $\mathcal{O}(M)$  ( $M$  being the number of intersection points, i.e., vertices of the jet cores), yielding a total detection complexity of  $\mathcal{O}(\sqrt{N} + M)$ .

We have measured the performance of a CPU implementation of our detection algorithm in Met.3D [38] on a desktop computer equipped with an Intel Core i7 3770 processor with 4.0 GHz  $\times$  4 cores, 32 GB RAM and an NVIDIA Geforce GTX 970. For an ENS forecast with a grid spacing of  $1^\circ$  in both latitude and longitude and a grid size of  $131 \times 66 \times 70$  cells, the isosurface intersection step took less than 300 ms for each single member of the 51 ensemble members. Core line filtering was performed on average in about 140 ms per member. A larger grid with a horizontal grid spacing of  $0.15^\circ$  and  $268 \times 669 \times 72$  cells required about 5 s for the isosurface intersection and 1.3 s for filtering.

## 4 VISUALIZATION TECHNIQUES

We have designed a number of visualization techniques to facilitate improved visual analysis of the detected 3D jet-stream cores in both 2D and 3D space. Our techniques support domain experts in their analysis and provide answers to important questions concerning jet cores: specifically their 3D shape, the strength of the wind along them, their orientation in relation to the wind direction, and their elevation.

### 4.1 Jet Core Rendering

Core line geometry is rendered in 2D and 3D as tubes. Fig. 4 shows how arrow glyphs placed at the end of each jet core line indicate their orientation; core line parameters can be encoded via tube thickness and color. This facilitates the simultaneous visualization of, (e.g.) wind speed and pressure elevation or flight level. For example, in Fig. 4, wind speed is mapped to tube thickness and pressure to color; the core lines are mainly located at pressure elevations between 200 and 300 hPa. Thin lines represent cores of weak wind speeds and likely small impact, whereas thick lines depict cores of potentially high impact.

Fig. 5 shows a 3D visualization, displaying the full 3D structure of the core lines. Notably, this 3D structure cannot be communicated via standard SIGWX charts. Since spatial perception in 3D renderings is crucial to meteorological analyses (cf. [38]), we render tube shadows cast by a directional light source from above onto the surface to show the horizontal location of the core lines. Based on feedback from

domain experts in our author team, we additionally provide drop-lines to further improve spatial perception in the vertical. The drop-lines are vertical axes connecting the core line with the surface, placed at the endpoints of each core line. They are augmented by text-labeled tick marks at user-defined pressure levels to display quantitative elevation information (Fig. 5).

### 4.2 Jet Cores in Atmospheric Flow

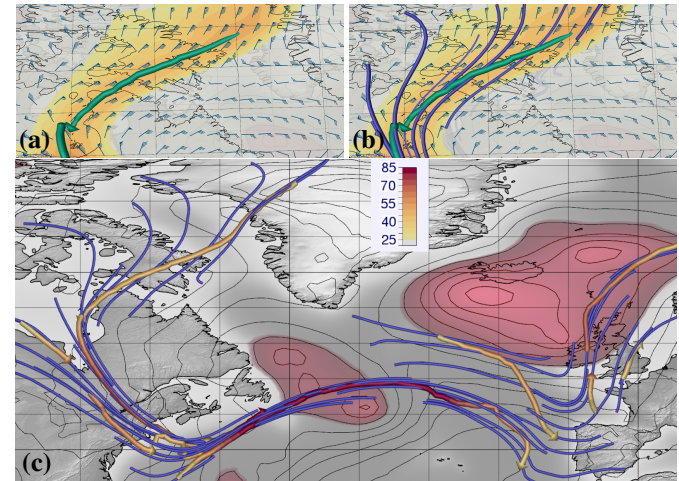


Fig. 6. Visualization of a jet-stream core line (green) and a horizontal section of the wind speed field (color in  $\text{ms}^{-1}$ ), (a) in combination with wind barbs, (b) with additional blue-colored streamlines, seeded along the core line at a fixed interval, and (c) all jet core lines and their streamlines, with MSLP as in Fig. 5, over the North Atlantic. Such displays can help scientists to analyze the jet core orientation relative to the flow direction. In some locations the angle between the two is small, indicating that little lateral movement of the core is expected in the near future (e.g., east of Newfoundland), whereas in others the angle is large, suggesting jet core movement (e.g., near to and south-west of Ireland, where a trough and jet cores on its forward and rearward flanks are all moving east-northeast).

Jet-streams follow the large-scale, moving wave patterns in the atmosphere. Newton and Omoto [33] showed that due to energy considerations in a moving wave system, the jet-stream core line must meander across the flow's streamlines; the jet-stream wave can only move if there is a wind component normal to the core (cf. Fig. 11 in [33]), and indeed moves with a speed approximately equal to the jet-core-normal wind component. Equivalently, only in a stationary wave in which the jet core has a uniform speed is the core line expected to be everywhere tangential to the streamlines. To shed light on the strength of the meandering in real-world forecasts, and hence on the expected advection of a core with the wind, we provide options to visualize the cores in the surrounding flow field. The core lines can be embedded into visualizations using standard wind barbs (Fig. 6a) to provide map-based displays similar to those typically used in operational settings. Additionally, streamlines (started at intervals along the core) can highlight the deviation between the core and local flow direction (Fig. 6b and c).

Visualization of jet cores along with further atmospheric fields (Fig. 5 and Fig. 6b) provides entirely new possibilities to examine the relation of the cores to weather events of interest. For example, 2D surface fields including mean-sea-level pressure can be displayed as line and filled contours (Fig. 6b), whilst 3D fields including cloud water content can be visualized as 3D isosurfaces (Sect. 5.2). In such examples one can examine jet cores and their connection to cyclones and anticyclones, or the relationship of jet cores to extreme weather (such as heavy rain and strong surface winds).

### 4.3 Ensemble Uncertainty

The visualization techniques presented above show just a single forecast. In operational forecasting, ensembles of forecasts are in widespread use (e.g., [13]) and need to be analyzed to investigate the uncertainty represented by the forecasts. In particular, experts need to examine the variability and coherence of predicted weather conditions and, thus, with respect to our work, the spread of detected jet cores across all ensemble members.

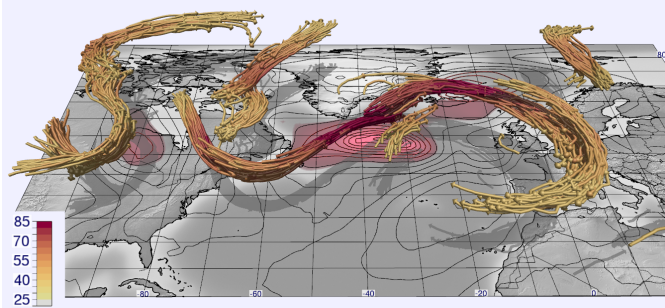


Fig. 7. 3D jet-stream core lines detected from the wind fields of 51 ensemble members of an ECMWF ENS forecast. Line color shows wind speed ( $\text{ms}^{-1}$ ), MSLP is rendered as in Fig. 5.

To support such analyses, we provide “spaghetti plots”, a simultaneous display of multiple members in a single image. Fig. 7 shows an example of a 3D spaghetti plot, including the core lines of all ensemble members of the considered forecast. The wider the jet cores are spread over the map, the more the forecast can be considered uncertain.

## 5 RESULTS

To demonstrate the value of our method, we discuss two applications. The first application demonstrates the automatic generation of jet-streams for a SIGWX product. The second case considers a real-world ensemble forecast from the recent North Atlantic Waveguide and Downstream Impact Experiment (NAWDEX, [9]), an atmospheric research field campaign involving one of the authors. The analysis of ensemble behavior during the campaign cases is a major focus of the –at the time of writing ongoing– data analysis activities of the campaign.

### 5.1 Significant Weather Charts

Jet cores are marked as one component on official medium and high level SIGWX (significant weather) charts prepared for aviation purposes by meteorologists, following regulations of the International Civil Aviation Organization [17]. In practice, forecasters at the UK Met Office, one of the two world area forecast centers (WAFCs), perform this manually, broadly as follows (pers. comm., P. McGarry and D. Naylor):

1. Examine 2-D fields of forecast maximum wind (in a vertical sense) depicted as isotachs (lines of constant wind speed) and vectors, supplemented by gridded wind data for various levels.
2. Draw jet core lines that broadly follow the speed maxima, but with a secondary consideration that the wind flags on the output chart, that by convention have to be shown parallel to the core line, do not depart too much from also being wind-parallel. Only include cores lines where wind speed exceeds 80 knots.
3. According to regulations in [17], add supplementary jet-related information, and also adjust to ensure correct prioritisation when depicting multiple hazards, and intelligibility for users - for example jet cores at two different levels cannot be overlaid.

Fig. 8 shows a comparison of an operationally issued SIGWX chart and jet-stream core lines detected by our approach; a second example is contained in Fig. 1. Having examined a number of cases we would describe the agreement between the SIGWX and our plots as very good. The main reasons for any discrepancies are as follows:

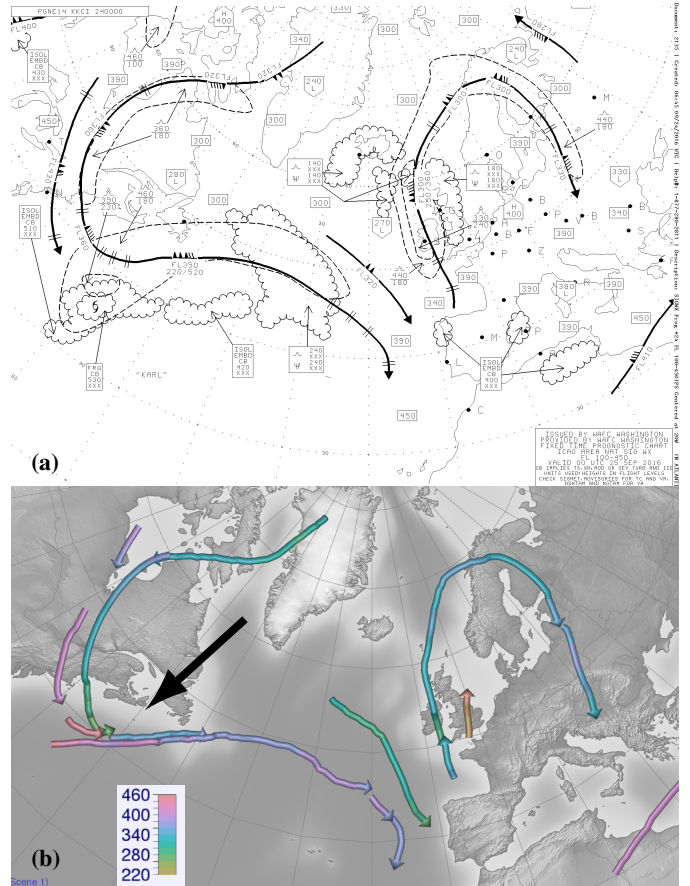


Fig. 8. Comparison of jet-stream core lines (a) manually identified by forecasters on operational significant weather charts, shown as thick solid arrows, with FLxxx notation alongside wind flags denoting flight level (xxx in hft), and (b) automatically detected by our method, colored by flight level (hft). Charts are valid at 00:00 UTC 25 September 2016; core lines in (a) are based on various forecast models available to the forecasters, those in (b) are based on the control analysis of the ECMWF ensemble forecast.

- “Artistic licence” by the SIGWX chart analyst, who has to combine multiple features intelligibly, with prioritisation, on their chart, abiding also by some official rules regarding overlaps.
- Differences in interpretation of available data between analysts (i.e., two forecasters given the same data would not produce the same chart).

In Fig. 8, the area south of Nova Scotia (black arrow in Fig. 8b) is interesting. Whilst our automated method picks out distinct jet cores at multiple levels (Fig. 8b), the manual method simplifies, showing just one jet core at 36000 ft (FL360), with a deep region of turbulence (FL180 to FL460, within the dashed line) probably added to cater for the multiple jets (Fig. 8a). Perhaps using our products the jet could be have been consigned to a more appropriate, lower level, and the turbulence region made more confined. Indeed we received the following general comment: “more information over the shape of the jets and potentially where they overlap could allow for more intelligent route planning to avoid turbulence/increase efficiencies” (pers. comm., S. Ramsdale, Chief Forecaster at the UK Met Office).

Thus our new 3D jet products can be used as helpful first guess fields to be rationalised by the SIGWX analysts. Overlapping jets, which are important and relatively frequent (see Sect. 5.2 below), are missing on the “wind maximum” field used in step 1 above, but with our method would be very visible.

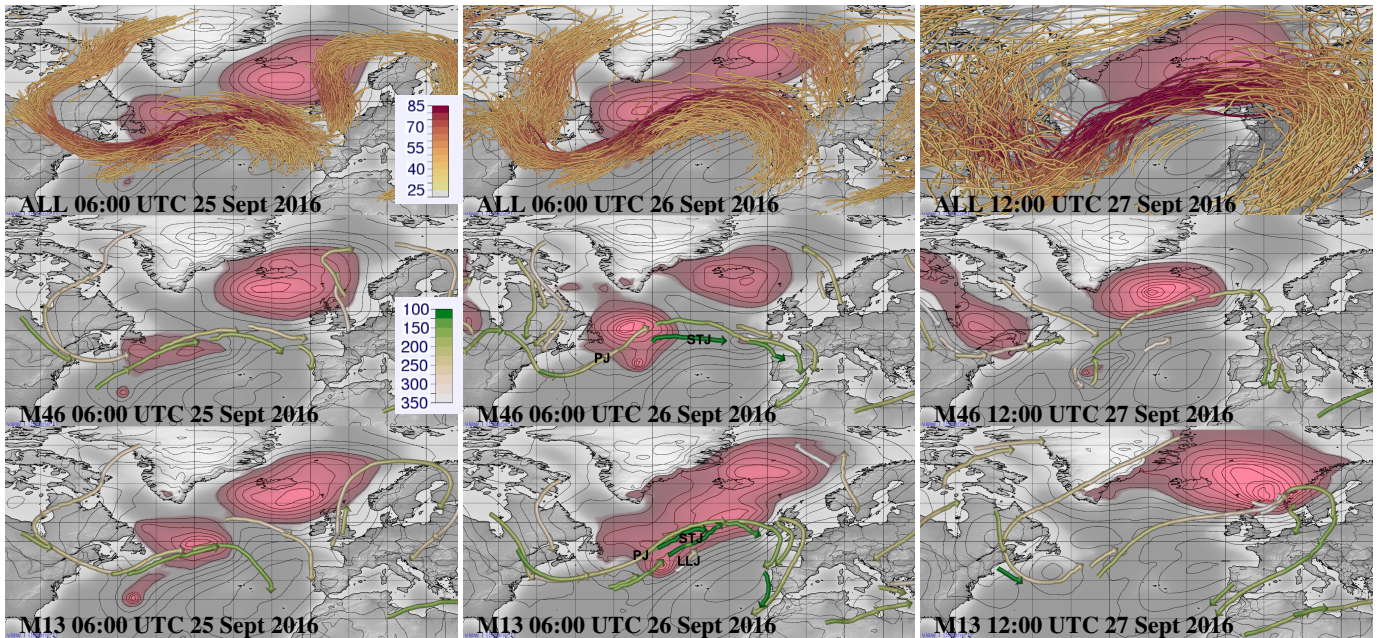


Fig. 9. Top row: “Spaghetti” representation of jet-stream core lines detected from the ECMWF ensemble forecast from 00:00 UTC 22 September 2016, valid at the indicated times. Jet-stream core lines are colored by wind speed ( $\text{ms}^{-1}$ ), contours and red shading show sea level pressure (red shading indicates pressure below 1000 hPa). Middle and bottom rows: Temporal development (same time steps) in two selected members (M46 and M13). Jet-stream core lines are colored by pressure elevation (hPa). In M13, a strong cyclone develops that on 27 September hits Norway. Annotation on central panels relates to jet types; PJ for polar Jet, STJ for sub-tropical jet, LLJ for low-level jet (used also on Fig. 10).

## 5.2 Tropical Cyclone “Karl”

We consider a real-world case from the NAWDEX campaign that represents applications in both weather forecasting and atmospheric research into physical processes. The extratropical transition of Tropical Cyclone Karl occurred in late September 2016. The system was successfully observed in multiple research flights, but had posed significant difficulties for forecasting due to associated high uncertainty.

We focus on the ECMWF ensemble starting from 00:00 UTC 22 September 2016, and specifically on the behavior of Karl as it became an extra-tropical feature in those forecasts. The ensemble included very different outcomes. These outcomes are analyzed in relation to detected jet-stream cores. We show how identifying the 3D cores facilitates investigation of jet behavior in a way not possible with classical wind speed analysis at single levels.

The top row in Fig. 9 shows a spaghetti representation of jet cores in the ensemble, on 3 different days, with the ensemble mean surface pressure field (MSLP). Spread increases quite dramatically with time (in surface weather too, not shown). However the salient features remain clear, most notably the eastward migration of a strong jet (darker reds on core lines) into the mid Atlantic. Karl is visible on the first frame, in the MSLP field due south of Newfoundland, but then moves northeast beneath the jet(s), to potentially interact with them.

We illustrate two very different ways in which that jet interaction could have played out, using two ensemble members denoted M13 and M46. Plan view time series of jet cores and surface pressure for each are depicted in Fig. 9. Greens denote jet core altitude, darker being higher (pressure level in hPa on scale). We can see three types of jet, a polar jet (PJ) at high levels, a subtropical jet (STJ) attributable in part to outflow from Karl, at very high levels (commensurate with tropical air), and in one case also a low level jet (LLJ) close to Karl’s center. Each jet may have more than one core. The behavior of the STJ relative to the PJ seems to play a pivotal role in determining subsequent evolution. Animation shows that the STJ in Fig. 9 (M46 06:00 UTC 26 Sept 2016) propagates rapidly forward away from Karl, turns anticyclonically, and reinforces the upper trough east of Iberia. Fig. 10a is a 3D view for 6h later – note how the high altitude STJ towers above other features, but is moving on, leaving the PJ behind. Conversely in Fig. 10b, 6h

after Fig. 9 (M13 06:00 UTC 26 Sept 2016), the three STJ branches do not propagate forwards, and indeed the westernmost STJ branch moves north to become vertically aligned with the two PJ branches, as can be seen in the shadows, and indeed on Fig. 10c where the added section shows wind speed. This vertical stacking is commensurate with a “tropopause wall” developing, which in energetic terms is very conducive to rapid cyclogenesis should a surface low, in this case Karl, happen to move poleward of the (stacked) jet cores.

In the M46 case Karl died, as can be inferred from Fig. 9, in part because the jet configuration did not help its development. However in the M13 case Karl crossed the cores and developed very rapidly, becoming a sub-970 hPa low center with extreme surface winds near Norway (cf. Fig. 9). Fig. 10d shows a rendering of the jet cores, cloud field and MSLP, 24 h after Fig. 10b and c. The STJ migrated east as the development ensued, the PJ is still very strong, with its left exit area near the low, assisting cyclogenesis. We also see a new mid level jet (MLJ) connecting up to the STJ (showing also that our code can identify altitude changes in jet level well). In addition there are two new LLJ cores at low levels. The lower one of these begins around 800 hPa, with hints of greater strength at its eastern end, reminiscent of the sting jet (SJ) phenomena implicated in many damaging European windstorms [6, 16], though further analysis would be needed to prove this connection.

We have seen that jet behavior is pivotal in this example, notably for the STJ. Further related research can focus on the role moist processes (for example) play in dictating jet behavior, which in turn feeds back on synoptic evolution. Other aspects that this case usefully reveals, also worthy of further study, are the mid level jet on Fig. 10d, and its upward connection, and the trough extension effect of the STJ in Fig. 10a. Thus 3D jet identification can highlight in a particularly compact and illuminating way new aspects of atmospheric structure that can be missed by classical 2D analysis methods.

Furthermore, regarding forecasting applications, domain expert S. Ramsdale (UK Met Office, pers. comm.) comments: “your approach...could be easily extended to show interactions between upper/surface level features in terms of perhaps vertical velocity around the cores, showing their penetration depth for development, allowing

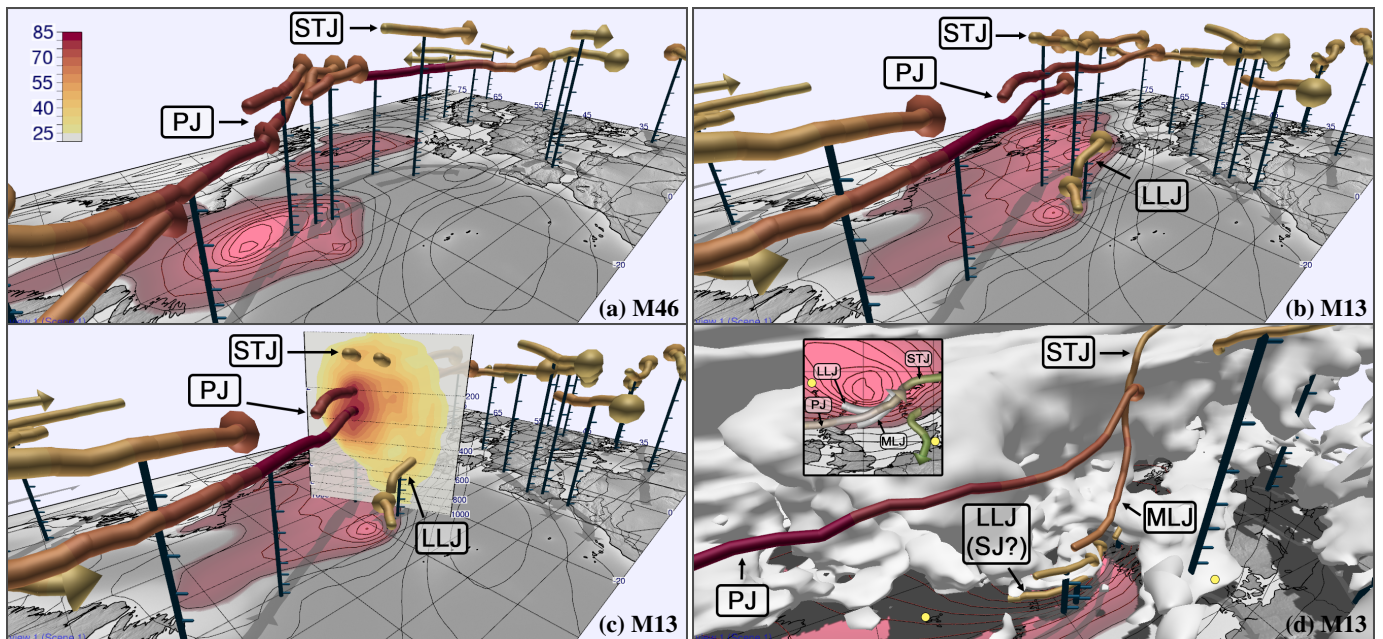


Fig. 10. Application of the proposed visualizations to the analysis of the extra-tropical transition of Tropical Cyclone Karl. Jet-stream core lines detected in the ECMWF ensemble forecast from 00:00 UTC 22 September 2016, valid 12:00 UTC 26 September 2016. Core lines are colored by wind speed ( $\text{ms}^{-1}$ ), contours show sea level pressure (red shading indicates pressure below 1000 hPa): (a) 3D view for member 46, (b) 3D view for member 13, (c) The same as (b) but with an added vertical section colored by wind speed, (d) 3D structure of member 13 off the coast of Norway, valid 12:00 UTC 27 September 2016. White isosurface encloses cloud cover fraction larger than 0.55. Inset, for same time, extracted from lower right panel of Fig 9. Yellow dots (at sea level) added to aid registration.

for again more objective assessments of how differences in shape/speed may lead to differences in evolution”. In addition he highlights the utility, for forecasting purposes, of real-time comparison of observations (e.g. winds from aircraft) with our jet cores.

For future research, one other area to highlight in which application of our method will be of interest is ‘forecast failures’. Rodwell et al. [41] found that these often stem from modulation of downstream flow, and notably upper level jets, by mishandled convective outbreaks over North America. Our new tools will highlight the upscale effects of such convective errors in revealing ways, with spaghetti jet plots for example (see Fig. 9) likely to yield key insights in a fraction of the time it would ordinarily take to examine all ensemble members.

## 6 CONCLUSION

We have proposed a robust detection method for identifying jet-stream core lines in atmospheric flow, and have presented visualization techniques that facilitate analysis of 3D jet-stream behavior in a way not possible with classical meteorological wind speed analysis at single vertical levels. Our method is to some extent similar to 3D height ridge detection but exploits wind direction information to achieve increased stability and greater agreement with classical manual detection methods. We have developed our methodology within a team of visualization and atmospheric scientists, have demonstrated how the method behaves when fed with realistic wind fields from numerical weather forecasts, and have proposed 2D and 3D visualization techniques.

Detection and visualization has been incorporated into the open-source meteorological 3D ensemble visualization tool “Met.3D” to facilitate combination of the new jet features with visualization of other important meteorological phenomena, and in order to promulgate the general methodology into the meteorological community. We have demonstrated how our method supports analysis that relies on core line geometry, including investigation of core line relationship to streamlines and investigation of jet core uncertainty inherent in ensemble weather prediction.

Two case studies have highlighted the value of our method for meteorological applications. We examined the automatic identification

of jet-stream core lines for global SIGWX charts used worldwide in aviation, and we examined closely the 3D jet-stream behavior during a specific weather case involving the extratropical transition of Tropical Cyclone Karl.

In conclusion, we are confident that our method will facilitate many new and valuable studies in atmospheric research, and that it will bring important benefits to operational weather forecasting. In our case study we have already identified interesting 3D jet-stream structures that are very relevant for whether or not extreme and damaging weather will develop at the surface. We are confident this will stimulate further meteorological research that addresses societal needs. Above all, we have achieved for the first time a compact, smooth, continuous 3D depiction of one of the most fundamental atmospheric features—the jet stream—that plays a pivotal role in determining world weather, and that even achieves frequent references in the media.

## ACKNOWLEDGMENTS

The research leading to these results has been done within the subproject “Visualization of coherence and variation in meteorological dynamics” of the Transregional Collaborative Research Center SFB/TRR 165 “Waves to Weather” funded by the German Research Foundation (DFG). The work was partly funded by the European Union under the ERC Advanced Grant 291372 SaferVis: Uncertainty Visualization for Reliable Data Discovery. Access to ECMWF prediction data has been kindly provided in the context of the ECMWF special project “Support Tool for HALO Missions”.

## REFERENCES

- [1] C. L. Archer and K. Caldeira. Historical trends in the jet streams. *Geophys. Res. Lett.*, 35(8):L08803+, Apr. 2008.
- [2] C. Baehr, B. Pouponneau, F. Ayrault, and A. Joly. Dynamical characterization of the FASTEX cyclogenesis cases. *Q.J.R. Meteorol. Soc.*, 125(561):3469–3494, Oct. 1999.
- [3] N. P. Barton and A. W. Ellis. Variability in wintertime position and strength of the North Pacific jet stream as represented by re-analysis data. *Int. J. Climatol.*, 29(6):851–862, May 2009.

- [4] G. Berry, C. Thorncroft, and T. Hewson. African easterly waves during 2004—Analysis using objective techniques. *Mon. Wea. Rev.*, 135(4):1251–1267, Apr. 2007.
- [5] D. C. Breton. Note sur les lignes de faite et de thalweg. *Comptes rendus hebdomadaires des séances de l'académie des Sciences*, 39:647–648, 1854.
- [6] K. A. Browning. The sting at the end of the tail: damaging winds associated with extratropical cyclones. *Q.J.R. Meteorol. Soc.*, 130(597):375–399, Jan. 2004.
- [7] K. A. Browning and N. M. Roberts. Structure of a frontal cyclone. *Q.J.R. Meteorol. Soc.*, 120(520):1535–1557, Oct. 1994.
- [8] M. de Saint-Venant. Surfaces à plus grande pente constituées sur des lignes courbes. *Bulletin de la Société Philomathématique de Paris*, pp. 24–30, 1852.
- [9] Deutsches Zentrum für Luft- und Raumfahrt. NAWDEX - North Atlantic Waveguide and Downstream Impact Experiment. <http://www.pa.op.dlr.de/nawdex>, 2016. Accessed 26 July 2017.
- [10] D. Eberly, R. Gardner, B. Morse, S. Pizer, and C. Scharlach. Ridges for image analysis. *Journal of Mathematical Imaging and Vision*, 4(4):353–373, 1994.
- [11] J. D. Furst and S. M. Pizer. Marching ridges. In M. H. Hamza, ed., *SIP*, pp. 22–26. IASTED/ACTA Press, 2001.
- [12] D. Gallego, P. Ribera, R. Garcia-Herrera, E. Hernandez, and L. Gimeno. A new look for the southern hemisphere jet stream. *24(6):607–621*, 2005.
- [13] T. Gneiting and A. E. Raftery. Weather forecasting with ensemble methods. *Science*, 310(5746):248–249, 2005.
- [14] R. M. Haralick. Ridges and valleys on digital images. *Computer Vision, Graphics, and Image Processing*, 22(1):28 – 38, 1983.
- [15] T. D. Hewson. Objective fronts. *Met. Apps*, 5(1):37–65, 1998.
- [16] T. D. Hewson and U. Neu. Cyclones, windstorms and the IMILAST project. *Tellus A: Dynamic Meteorology and Oceanography*, 67(1):27128+, Jan. 2015.
- [17] International Civil Aviation Organization. *Meteorological Service for International Air Navigation, Annex 3 to the Convention on International Civil Aviation*. International Civil Aviation Organization, 999 University Street, Montréal, Quebec, Canada H3C 5H7, 17th ed., 2010.
- [18] D. N. Kenwright, C. Henze, and C. Levit. Feature extraction of separation and attachment lines. *IEEE Transactions on Visualization and Computer Graphics*, 5(2):135–144, 1999.
- [19] G. Kindlmann. Semi-automatic generation of transfer functions for direct volume rendering. Master's thesis, Cornell University, USA, 1999.
- [20] P. Koch, H. Wernli, and H. C. Davies. An event-based jet-stream climatology and typology. *Int. J. Climatol.*, 26(3):283–301, 2006.
- [21] M. Leutbecher and T. Palmer. Ensemble forecasting. *J. Comput. Phys.*, 227(7):3515–3539, Mar. 2008.
- [22] Y. Levy, D. Degani, and A. Seginer. Graphical visualization of vortical flows by means of helicity. *AIAA*, 28(8):1347–1352, 1990.
- [23] S. Limbach, E. Schömer, and H. Wernli. Detection, tracking and event localization of jet stream features in 4-D atmospheric data. *Geosci. Model Dev.*, 5(2):457–470, Apr. 2012.
- [24] T. Lindeberg. Edge detection and ridge detection with automatic scale selection. *30(2):117–156*, 1998.
- [25] P. Ljung and A. Ynnerman. Extraction of intersection curves from iso-surfaces on co-located 3D grids. In *The Annual SIGRAD Conference. Special Theme - Real-Time Simulations. Conference Proceedings from SIGRAD2003*, number 10, pp. 23–28. Linköping University Electronic Press; Linköpings universitet, 2003.
- [26] W. E. Lorensen and H. E. Cline. Marching cubes: A high resolution 3D surface construction algorithm. In *Proceedings of the 14th Annual Conference on Computer Graphics and Interactive Techniques*, vol. 21 of *SIGGRAPH '87*, pp. 163–169. ACM, New York, NY, USA, July 1987.
- [27] G. M. Machado, F. Sadlo, and T. Ertl. Local extraction of bifurcation lines. In *Proceedings of International Workshop on Vision, Modeling and Visualization (VMV)*, pp. 17–24, 2013.
- [28] P. Majer. *A statistical approach to feature detection and scale selection in images*. Niedersächsische Staats-und Universitätsbibliothek, 2000.
- [29] G. L. Manney, M. I. Hegglin, W. H. Daffer, M. L. Santee, E. A. Ray, S. Pawson, M. J. Schwartz, C. D. Boone, L. Froidevaux, N. J. Livesey, W. G. Read, and K. A. Walker. Jet characterization in the upper troposphere/lower stratosphere (UTLS): applications to climatology and transport studies. *Atmospheric Chemistry and Physics*, 11(12):6115–6137, June 2011.
- [30] G. L. Manney, M. I. Hegglin, W. H. Daffer, M. J. Schwartz, M. L. Santee, and S. Pawson. Climatology of upper Tropospheric–Lower stratospheric (UTLS) jets and tropopause in MERRA. *J. Climate*, 27(9):3248–3271, Jan. 2014.
- [31] O. Martius. A Lagrangian analysis of the northern hemisphere subtropical jet. *J. Atmos. Sci.*, 71(7):2354–2369, Mar. 2014.
- [32] S. Molnos, T. Mamdouh, S. Petri, T. Noeke, T. Weinkauff, and D. Coumou. A network-based detection scheme for the jet stream core. *Earth System Dynamics*, 8(1):75–89, Feb. 2017.
- [33] C. W. Newton and Y. Omoto. Energy distribution near jet stream, and associated wave-amplitude relations. *Tellus*, 17(4):449–462, Nov. 1965.
- [34] E. Palmén and C. W. Newton. *Atmospheric circulation systems: their structure and physical interpretation (International Geophysics)*. Academic Press, Aug. 1969.
- [35] R. Peikert and F. Sadlo. Height ridge computation and filtering for visualization. In *2008 IEEE Pacific Visualization Symposium*, pp. 119–126, March 2008.
- [36] C. Pena-Ortiz, D. Gallego, P. Ribera, P. Ordonez, and M. D. Alvarez-Castro. Observed trends in the global jet stream characteristics during the second half of the 20th century. *J. Geophys. Res. Atmos.*, 118(7):2702–2713, Apr. 2013.
- [37] A. Persson and E. Andersson. *User guide to ECMWF forecast products, version 1.1*. European Centre for Medium-Range Weather Forecasts (ECMWF), Reading, UK, 2013.
- [38] M. Rautenhaus, M. Kern, A. Schäfler, and R. Westermann. Three-dimensional visualization of ensemble weather forecasts – Part 1: The visualization tool Met.3D (version 1.0). *Geosci. Model Dev.*, 8(7):2329–2353, 2015.
- [39] E. R. Reiter. *Jet-stream meteorology*. University of Chicago Press, 1st ed.
- [40] L. Rikus. A simple climatology of westerly jet streams in global reanalysis datasets part 1: mid-latitude upper tropospheric jets. pp. 1–26, 2015.
- [41] M. J. Rodwell, L. Magnusson, P. Bauer, P. Bechtold, M. Bonavita, C. Cardinali, M. Diamantakis, P. Earnshaw, A. Garcia-Mendez, L. Isaksen, E. Källén, D. Klocke, P. Lopez, T. McNally, A. Persson, F. Prates, and N. Wedi. Characteristics of occasional poor medium-range weather forecasts for Europe. *Bull. Amer. Meteor. Soc.*, 94(9):1393–1405, Feb. 2013.
- [42] M. Roth. *Automatic Extraction of Vortex Core Lines and Other Line-Type Features for Scientific Visualization*. PhD thesis, Swiss Federal Institute of Technology, ETH Zürich, 2000.
- [43] F. Sadlo and R. Peikert. Efficient visualization of Lagrangian coherent structures by filtered AMR ridge extraction. *IEEE Transactions on Visualization and Computer Graphics*, 13(6):1456–1463, Nov 2007.
- [44] J. Sahner, T. Weinkauff, N. Teuber, and H. C. Hege. Vortex and strain skeletons in Eulerian and Lagrangian frames. *IEEE Transactions on Visualization and Computer Graphics*, 13(5):980–990, Sept 2007.
- [45] R. Schiemann, D. Lüthi, and C. Schär. Seasonality and interannual variability of the westerly jet in the Tibetan plateau region. *J. Climate*, 22(11):2940–2957, June 2009.
- [46] S. C. Shadden, F. Lekien, and J. E. Marsden. Definition and properties of Lagrangian coherent structures from finite-time Lyapunov exponents in two-dimensional aperiodic flows. *Physica D: Nonlinear Phenomena*, 212(3-4):271 – 304, 2005.
- [47] C. Spensberger, T. Spenger, and C. Li. Upper tropospheric jet axis detection and application to the boreal winter 2013/14. *Mon. Wea. Rev.*, Mar. 2017.
- [48] R. C. Strawn, D. N. Kenwright, and J. Ahmad. Computer visualization of vortex wake systems. *AIAA journal*, 37(4):511–512, 1999.
- [49] C. Strong and R. E. Davis. The surface of maximum wind as an alternative to the isobaric surface for wind climatology. *Geophys. Res. Lett.*, 32(4):L04813+, Feb. 2005.
- [50] C. Strong and R. E. Davis. Winter jet stream trends over the northern hemisphere. *Q.J.R. Meteorol. Soc.*, 133(629):2109–2115, Oct. 2007.
- [51] C. Strong and R. E. Davis. Variability in the position and strength of winter jet stream cores related to northern hemisphere teleconnections. *J. Climate*, 21(3):584–592, Feb. 2008.
- [52] D. Sujudi and R. Haimes. Identification of swirling flow in 3D vector fields. In *19th AIAA Computational Fluid Dynamics Conference*, pp. 95–1715, 1995.
- [53] C. Tyson and M. Strahan. *Representing WAFS Significant Weather (SIGWX) Data in BUFR, Version 4.3*. World Area Forecast Centres (WAFSCs), London and Washington, 2013.
- [54] World Meteorological Organization. *International Meteorological Vocabulary*. WMO. WMO, 2nd ed., 1992.